Civil Engineering Infrastructures Journal, 46(1): 1 – 14, June 2013
ISSN: 2322 – 2093

Analytical Solution for a Two-Layer Transversely Isotropic Half-Space Affected by an Arbitrary Shape Dynamic Surface Load

Ardeshir-Behrestaghi, A.[1] , Eskandari-Ghadi, M.[2*] and Vaseghi-Amiri, J.[3]

[1] PhD Candidate, Faculty of Civil Engineering, Babol Noshirvani University of Technology, Babol, Iran.
[2] Associate Professor, School of Civil Engineering, College of Engineering, University of Tehran, P.O.Box: 11155-4563, Tehran, Iran.
[3] Associate Professor, Faculty of Civil Engineering, Babol Noshirvani University of Technology, Babol, Iran.

Received: 9 Apr. 2011; Revised: 12 Oct. 2011; Accepted: 10 Mar. 2012

ABSTRACT: The dynamic response of a transversely isotropic, linearly elastic layer bonded to the surface of a half-space of a different transversely isotropic material under arbitrary shape surface loads is considered. With the help of displacements and stresses Green's functions, an analytical formulation is presented for the determination of the displacements and stresses at any point in both surface layer and the underneath half-space in frequency domain. Special results are prepared for circular, ellipsoidal, square and recangular patch load. It is shown that the displacements and stresses due to circular patch load are colapesd on the existing solution in the literature. Some new illustrations are prepared to show the effect of the shape of the patch on the responses of the domain specially near the load.

Keywords: Forced Vibration, Layer Medium, Solid Mechanics, Transversely Isotropic, Wave Propagation.

INTRODUCTION

The determination of the response of a solid medium under a dynamic load has significant interest in the mathematical as well as applied theory of elasticity. In engineering, such problems are relevant to foundation engineering and compaction control in geotechnical engineering, as examples. The circular geometry of the loaded area, full or annulus contact, is less complicated than other shape loaded area, and thus has been more interested in the literature for understanding the mechanical behavior of the problem (Harding and Sneddon, 1945; Egorov, 1965; Keer, 1967; Dhawan, 1979; Tassoulas and Kausel, 1984; Johnson, 1986; Kim et al., 1987; Veletsos, 1987; Shield and Bogy, 1989; Melerski, 1997; Guzina and Nintcheu, 2001; Pak et al., 2008; Eskandari-Ghadi et al., 2009 and 2010). However, other shapes like square, rectangle and elliptic are being the most common shapes for foundation and thus are of more engineering applications (Wong and Trifunac, 1974; Wong and Luco, 1975; Bycroft, 1980; Iguchi and Luco, 1980; Mita and Luco, 1989; Veletsos and Prasad, 1996;

* Corresponding author E-mail: ghadi@ut.ac.ir

Ahmad, and Rupani, 1999; Algin, 2000; Kenzo, 2000). A domain may be affected by a patch load or a rigid solid, and both cases result in a complex problem. If an elastic isotropic or orthotropic half-space is affected by a rigid solid, and if an integral transform is used to solve the partial differential equations, then a dual integral equation is encountered. Because of the complexity of the procedure for obtaining analytical solution, an approximate numerical procedure for calculation of the harmonic force-displacement relationships for a rigid foundation of arbitrary shape placed on an elastic isotropic half-space was presented by Wong and Loco (1975). The procedure presented by Wong and Loco (1975) was used to evaluate the vertical, rocking and horizontal compliance functions for rigid rectangular foundations and the vertical compliance for a rigid square foundation with an internal hole.

Iguchi and Luco (1980) developed an approximate method for the analysis of the dynamic interaction between a flexible rectangular foundation and the soil with consideration of the out-of-plane deformation of the foundation. The procedure presented by Iguchi and Luco is based on an extension of the subdivision method developed by Wong and Luco (1975) for rigid foundations. Bycroft (1980) developed a general method for determining the motion of a large rigid mat foundation subjected to traveling surface waves.

In their paper, Mita and Luco (1989) used a hybrid approach to obtain the dynamic response of rigid square foundations embedded in an isotropic elastic half-space. The results are presented for excitations in the form of external forces and moments as well as for the case of plane elastic waves impinging on the foundation from different angles.

Ahmad and Rupani (1999) investigated into the influence of mechanical and geometrical parameters on the horizontal impedance of square foundations resting on or embedded in a two-layer isotropic soil deposit. The parameters investigated are the ratio of shear-wave velocities, the thickness of the top layer, the depth of embedment and the degree of contact between the footing-sidewall with backfill-soil. Algin (2000) presented a general algebraical formula, obtained by the integration of the Boussinesq equation, to determine the vertical stresses resulting from a linearly distributed surface pressure resting on an elastic isotropic medium. This problem and its various derivations has received considerable attention because of its applications in foundation engineering.

This kind of problem will be more complicated if the solid under the effect of the load is not isotropic. The most common anisotropic material used in engineering is transversely isotropic material. Eskandari-Ghadi et al. (2009) presented an analytical solution for the displacements and stresses of a transversely isotropic half-space affected by a vertically excited rigid circular foundation. Eskandari-Ghadi and Ardeshir-Behrestaghi (2010) developed the solution for the axisymmetric vertically motion induced in a transversely isotropic full-space by a rigid circular plate.

In this paper, a transversely isotropic layer bonded on the top of a half-space containing a different transversely isotropic material is considered as the domain of the problem. This domain is affected by a time harmonic arbitrary shape surface time harmonic load. The dynamic response of the domain is analytically investigated with the help of displacements and stresses Green's functions introduced in (Eskandari-Ghadi et al., 2008). The displacements and stresses, are expressed in double integrals, where the integrands are the related Green's functions. In spite of the poles and branch points in the path of integration, the integrals are

numerically evaluated with a very precise manner, so that the results are collapsed on the existing solution for the circular loaded area. Further results are presented for the square, rectanglar and elliptical shapes of loaded area, which can be used as benchmarks for foundation engineering in transversely isotropic soil, and as a reference for future numerical analysis of foundation.

CONFIGURATION OF THE PROBLEM AND IT'S GENERAL SOLUTION

A horizontal layer contains of a transversely isotropic linear elastic material bonded on the top of a half-space containing a transversely isotropic linear elastic material with different properties is considered as the domain of the problem. The axes of symmetry of both media are considered to be normal to the horizontal surface and thus parallel to each other. As indicated in Figure 1, a cylindrical coordinate system {O; $\boldsymbol{x}$ =(r, θ, z)} whose z-axis is in the depth-wise direction with respect to the layer and the half-space is used. As references, the top layer and the half-space are referred to as Region I ($0 < z < s$) and Region II ($z > s$), respectively. In such a setting, the general equations of motion for transversely isotropic media in the absence of body forces are:

$$
\begin{aligned}
&A_{11}\left(\frac{\partial^2 u}{\partial r^2}+\frac{1}{r}\frac{\partial u}{\partial r}-\frac{u}{r^2}\right)+\frac{A_{11}-A_{12}}{2}\frac{1}{r^2}\frac{\partial^2 u}{\partial \theta^2}+A_{44}\frac{\partial^2 u}{\partial z^2}\\
&+\frac{A_{11}+A_{12}}{2}\left(\frac{1}{r}\frac{\partial^2 v}{\partial r\partial \theta}+\frac{1}{r^2}\frac{\partial v}{\partial \theta}\right)-2A_{11}\frac{1}{r^2}\frac{\partial v}{\partial \theta}\\
&\qquad+(A_{13}+A_{44})\frac{\partial^2 w}{\partial r\partial z}=\rho\frac{\partial^2 u}{\partial t^2}\\
&\frac{A_{11}-A_{12}}{2}\left(\frac{\partial^2 v}{\partial r^2}+\frac{1}{r}\frac{\partial v}{\partial r}-\frac{v}{r^2}\right)+A_{11}\frac{1}{r^2}\frac{\partial^2 v}{\partial \theta^2}+A_{44}\frac{\partial^2 v}{\partial z^2}\\
&+\frac{A_{11}+A_{12}}{2}\left(\frac{1}{r}\frac{\partial^2 u}{\partial r\partial \theta}-\frac{1}{r^2}\frac{\partial u}{\partial \theta}\right)+2A_{11}\frac{1}{r^2}\frac{\partial u}{\partial \theta}\\
&\qquad+(A_{13}+A_{44})\frac{1}{r}\frac{\partial^2 w}{\partial \theta\partial z}=\rho\frac{\partial^2 v}{\partial t^2}\\
&A_{33}\frac{\partial^2 w}{\partial z^2}+A_{44}\left(\frac{\partial^2 w}{\partial r^2}+\frac{1}{r}\frac{\partial w}{\partial r}+\frac{1}{r^2}\frac{\partial^2 w}{\partial \theta^2}\right)\\
&\quad+(A_{13}+A_{44})\left(\frac{\partial^2 u}{\partial r\partial z}+\frac{1}{r}\frac{\partial u}{\partial z}+\frac{1}{r}\frac{\partial^2 v}{\partial \theta\partial z}\right)=\rho\frac{\partial^2 w}{\partial t^2}
\end{aligned}
\tag{1}
$$

where u, v and w are the displacement components in r-, θ- and z-direction, respectively; ρ is the material density, t denotes the time variable and A_{ij} are the elasticity constants in the stress strain relations, which can be found in (Lekhnitskii, 1981).

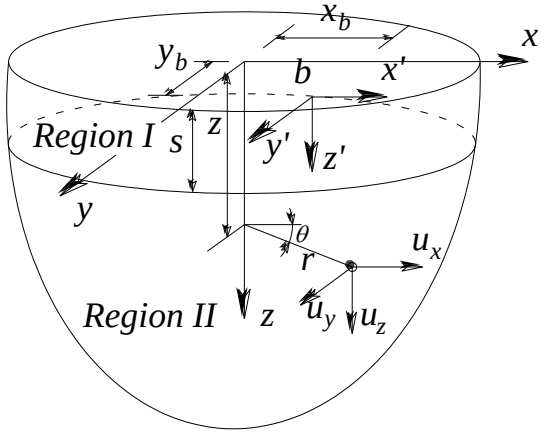

Fig. 1. Transversely isotropic layer (Region I) bonded on the top of a transversely isotropic half-space (Region II), system of reference and transformation of reference.

These elasticity constants, which are allowed to be different in Region I and II, are correlated to five engineering elastic constants, E, Young's modulus in the plane of transverse isotropy, E', Young's modulus in the plane perpendicular to plane of transverse isotropy, Poisson's ratios υ and υ' characterize the lateral strain response in the plane of transverse isotropy to a stress acting parallel and normal to it, G', the shear modulus in planes normal to the plane of transverse isotropy, and G, the shear modulus in the plane normal to the axis of symmetry and in the direction normal to it. In the case of isotropic material, the elasticity constants are as:

$$A_{11}=A_{33}=\lambda+2\mu,\ A_{12}=A_{13}=\lambda,\ A_{44}=A_{66}=\mu \tag{2}$$

where λ and μ are Lame's constants.

It is assumed that the set of the surface layer and the underneath half-space is under the effect of an arbitrary surface time-harmonic load applied on a plane π_0 at $z=0$. We denote the components of the surface traction as $P(r,\theta)$, $Q(r,\theta)$ and $R(r,\theta)$, which are applied in r-, θ- and z-direction, respectively, and $(r,\theta)\in\pi_0$. In addition, the vector of the total force applied on plane π_0 are denoted as $\mathbf{f}(r;\theta)=\boldsymbol{f}_v\,\mathbf{e}_z+\boldsymbol{f}_h\,\mathbf{e}_h$, where $\mathbf{e}_h=\mathbf{e}_r\cos\theta-\mathbf{e}_\theta\sin\theta$ and $\mathbf{e}_r,\mathbf{e}_\theta$ and $\mathbf{e}_z$ are the unit vector in r-, θ- and z-direction, respectively. In addition, $\boldsymbol{f}_h=\mathbf{e}_r\cos\theta\int_{\pi_0}P(r,\theta)\,dA-\mathbf{e}_\theta\sin\theta\int_{\pi_0}Q(r,\theta)\,dA$ and $\boldsymbol{f}_v=\mathbf{e}_z\int_{\pi_0}R(r,\theta)\,dA(r,\theta)$. Considering the boundary conditions at the surface of the half-space, the regularity condition at infinity, and the continuity condition at $z=s$, the displacements and stresses are written as bellow (Eskandari-Ghadi, et al., 2008) for region I:

$$\begin{aligned}
u_{1m}(r,z)=&-\frac{\alpha_{13}}{2}\int_0^\infty\xi^2\left[J_{m+1}(\xi r)-J_{m-1}(\xi r)\right]\\
&\times\Big[\lambda_{11}(A_{1m}e^{-\lambda_{11}z}-C_{1m}e^{\lambda_{11}z})\\
&+\lambda_{12}(B_{1m}e^{-\lambda_{12}z}-D_{1m}e^{\lambda_{12}z})\Big]d\xi\\
&-\frac{i}{2}\int_0^\infty\xi^2\left[J_{m+1}(\xi r)+J_{m-1}(\xi r)\right]\\
&\times\Big[G_{1m}e^{-\lambda_{13}z}+H_{1m}e^{\lambda_{13}z}\Big]d\xi\\
v_{1m}(r,z)=&\frac{i\alpha_{13}}{2}\int_0^\infty\xi^2\left[J_{m+1}(\xi r)+J_{m-1}(\xi r)\right]\\
&\times\Big[\lambda_{11}(A_{1m}e^{-\lambda_{11}z}-C_{1m}e^{\lambda_{11}z})\\
&+\lambda_{12}(B_{1m}e^{-\lambda_{12}z}-D_{1m}e^{\lambda_{12}z})\Big]d\xi\\
&-\frac{1}{2}\int_0^\infty\xi^2\left[J_{m+1}(\xi r)-J_{m-1}(\xi r)\right]\\
&\times\Big[G_{1m}e^{-\lambda_{13}z}+H_{1m}e^{\lambda_{13}z}\Big]d\xi\\
w_{1m}(r,z)=&\int_0^\infty\xi\Big[\varphi_{11}\left(A_{1m}e^{-\lambda_{11}z}+C_{1m}e^{\lambda_{11}z}\right)\\
&+\varphi_{12}\left(B_{1m}e^{-\lambda_{12}z}+D_{1m}e^{\lambda_{12}z}\right)\Big]J_m(\xi r)d\xi
\end{aligned} \tag{3}$$

$$\begin{aligned}
\sigma_{1zrm}(r,z)=&\frac{A_{144}}{2}\int_0^\infty\xi^2\Big[\eta_{11}(A_{1m}e^{-\lambda_{11}z}+C_{1m}e^{\lambda_{11}z})\\
&+\eta_{12}(B_{1m}e^{-\lambda_{12}z}+D_{1m}e^{\lambda_{12}z})\Big]\\
&\times\Big[J_{m+1}(\xi r)-J_{m-1}(\xi r)\Big]d\xi\\
&-\frac{A_{144}i}{2}\int_0^\infty\xi^2\lambda_{13}\Big[H_{1m}e^{\lambda_{13}z}-G_{1m}e^{-\lambda_{13}z}\Big]\\
&\times\Big[J_{m-1}(\xi r)+J_{m+1}(\xi r)\Big]d\xi\\
\sigma_{1z\theta m}(r,z)=&\frac{-A_{144}i}{2}\int_0^\infty\xi^2\Big[\eta_{11}(A_{1m}e^{-\lambda_{11}z}+C_{1m}e^{\lambda_{11}z})\\
&+\eta_{12}(B_{1m}e^{-\lambda_{12}z}+D_{1m}e^{\lambda_{12}z})\Big]\\
&\times\Big[J_{m+1}(\xi r)+J_{m-1}(\xi r)\Big]d\xi\\
&+\frac{A_{144}}{2}\int_0^\infty\xi^2\lambda_{13}\Big[H_{1m}e^{\lambda_{13}z}-G_{1m}e^{-\lambda_{13}z}\Big]\\
&\times\Big[J_{m-1}(\xi r)-J_{m+1}(\xi r)\Big]d\xi\\
\sigma_{1zzm}(r,z)=&A_{133}\int_0^\infty\xi\Big[\nu_{11}(A_{1m}e^{-\lambda_{11}z}-C_{1m}e^{\lambda_{11}z})\\
&+\nu_{12}(B_{1m}e^{-\lambda_{12}z}-D_{1m}e^{\lambda_{12}z})\Big]J_m(\xi r)\,d\xi
\end{aligned}$$

$$\sigma_{\mathrm{I}rrm}+(A_{111}-A_{112})\{(\frac{u_{1m}}{r})+im(\frac{v_{1m}}{r})\}=$$
$$-\int_0^\infty \xi\Big[\lambda_{11}(\alpha_{13}A_{111}\xi^2+A_{113}\varphi_{11})$$
$$\times(A_{1m}e^{-\lambda_{11}z}-C_{1m}e^{\lambda_{11}z})+\lambda_{12}(\alpha_{13}A_{111}\xi^2+A_{113}\varphi_{12})$$
$$\times(B_{1m}e^{-\lambda_{12}z}-D_{1m}e^{\lambda_{12}z})\Big]J_m(\xi r)\,d\xi$$
$$\sigma_{\mathrm{I}\theta\theta m}-(A_{111}-A_{112})\{(\frac{u_{1m}}{r})+im(\frac{v_{1m}}{r})\}=$$
$$-\int_0^\infty \xi\Big[\lambda_{11}(\alpha_{13}A_{112}\xi^2+A_{113}\varphi_{11})$$
$$\times(A_{1m}e^{-\lambda_{11}z}-C_{1m}e^{\lambda_{11}z})+\lambda_{12}(\alpha_{13}A_{112}\xi^2+A_{113}\varphi_{12})$$
$$\times(B_{1m}e^{-\lambda_{12}z}-D_{1m}e^{\lambda_{12}z})\Big]J_m(\xi r)\,d\xi$$
$$\sigma_{\mathrm{I}r\theta m}+(A_{111}-A_{112})\{(\frac{v_{1m}}{r})-im(\frac{u_{1m}}{r})\}=$$
$$-\frac{A_{111}-A_{112}}{2}\int_0^\infty \xi^3(H_{1m}e^{\lambda_{13}z}+G_{1m}e^{-\lambda_{13}z})J_m(\xi r)\,d\xi$$

(4)

and as follows for region II:

$$u_{\mathrm{II}m}(r,z)=-\frac{\alpha_{\mathrm{II}3}}{2}\int_0^\infty \xi^2\left[J_{m+1}(\xi r)-J_{m-1}(\xi r)\right]$$
$$\times\Big[\lambda_{\mathrm{II}1}A_{\mathrm{II}m}e^{-\lambda_{\mathrm{II}1}z}+\lambda_{\mathrm{II}2}B_{\mathrm{II}m}e^{-\lambda_{\mathrm{II}2}z}\Big]d\xi$$
$$-\frac{i}{2}\int_0^\infty \xi^2\left[J_{m+1}(\xi r)+J_{m-1}(\xi r)\right]G_{\mathrm{II}m}e^{-\lambda_{\mathrm{II}3}z}d\xi$$
$$v_{\mathrm{II}m}(r,z)=\frac{i\alpha_{\mathrm{II}3}}{2}\int_0^\infty \xi^2\left[J_{m+1}(\xi r)+J_{m-1}(\xi r)\right]$$
$$\times\Big[\lambda_{\mathrm{II}1}A_{\mathrm{II}m}e^{-\lambda_{\mathrm{II}1}z}+\lambda_{\mathrm{II}2}B_{\mathrm{II}m}e^{-\lambda_{\mathrm{II}2}z}\Big]d\xi$$
$$-\frac{1}{2}\int_0^\infty \xi^2\left[J_{m+1}(\xi r)-J_{m-1}(\xi r)\right]G_{\mathrm{II}m}e^{-\lambda_{\mathrm{II}3}z}d\xi$$
$$w_{\mathrm{II}m}(r,z)=\int_0^\infty \xi\Big[\varphi_{\mathrm{II}1}\,A_{\mathrm{II}m}e^{-\lambda_{\mathrm{II}1}z}$$
$$+\varphi_{\mathrm{II}2}\,B_{\mathrm{II}m}e^{-\lambda_{\mathrm{II}2}z}\Big]J_m(\xi r)d\xi$$

(5)

$$\sigma_{\mathrm{II}zrm}(r,z)=$$
$$\frac{A_{\mathrm{II}44}}{2}\int_0^\infty \xi^2\Big[\eta_{\mathrm{II}1}A_{\mathrm{II}m}e^{-\lambda_{\mathrm{II}1}z}+\eta_{\mathrm{II}2}B_{\mathrm{II}m}e^{-\lambda_{\mathrm{II}2}z}\Big]$$
$$\times\left[J_{m+1}(\xi r)-J_{m-1}(\xi r)\right]d\xi$$
$$+\frac{A_{\mathrm{II}44}i}{2}\int_0^\infty \xi^2\lambda_{\mathrm{II}3}G_{\mathrm{II}m}e^{-\lambda_{\mathrm{II}3}z}\left[J_{m-1}(\xi r)+J_{m+1}(\xi r)\right]d\xi$$
$$\sigma_{\mathrm{II}z\theta m}(r,z)=$$
$$\frac{-A_{\mathrm{II}44}i}{2}\int_0^\infty \xi^2\Big[\eta_{\mathrm{II}1}A_{\mathrm{II}m}e^{-\lambda_{\mathrm{II}1}z}+\eta_{\mathrm{II}2}B_{\mathrm{II}m}e^{-\lambda_{\mathrm{II}2}z}\Big]$$
$$\times\left[J_{m+1}(\xi r)+J_{m-1}(\xi r)\right]d\xi$$
$$-\frac{A_{\mathrm{II}44}}{2}\int_0^\infty \xi^2\lambda_{\mathrm{II}3}G_{\mathrm{II}m}e^{-\lambda_{\mathrm{II}3}z}\left[J_{m-1}(\xi r)-J_{m+1}(\xi r)\right]d\xi$$
$$\sigma_{\mathrm{II}zzm}(r,z)=A_{\mathrm{II}33}\int_0^\infty \xi\Big[\nu_{\mathrm{II}1}A_{\mathrm{II}m}e^{-\lambda_{\mathrm{II}1}z}$$
$$+\nu_{\mathrm{II}2}B_{\mathrm{II}m}e^{-\lambda_{\mathrm{II}2}z}\Big]J_m(\xi r)\,d\xi$$
$$\sigma_{\mathrm{II}rrm}+(A_{\mathrm{II}11}-A_{\mathrm{II}12})\{(\frac{u_{\mathrm{II}m}}{r})+im(\frac{v_{\mathrm{II}m}}{r})\}=$$
$$-\int_0^\infty \xi\Big[\lambda_{\mathrm{II}1}(\alpha_{\mathrm{II}3}A_{\mathrm{II}11}\xi^2+A_{\mathrm{II}13}\varphi_{\mathrm{II}1})A_{\mathrm{II}m}e^{-\lambda_{\mathrm{II}1}z}$$
$$+\lambda_{\mathrm{II}2}(\alpha_{\mathrm{II}3}A_{\mathrm{II}11}\xi^2+A_{\mathrm{II}13}\varphi_{\mathrm{II}2})B_{\mathrm{II}m}e^{-\lambda_{\mathrm{II}2}z}\Big]J_m(\xi r)\,d\xi$$
$$\sigma_{\mathrm{II}\theta\theta m}-(A_{\mathrm{II}11}-A_{\mathrm{II}12})\{(\frac{u_{\mathrm{II}m}}{r})+im(\frac{v_{\mathrm{II}m}}{r})\}=$$
$$-\int_0^\infty \xi\Big[\lambda_{\mathrm{II}1}(\alpha_{\mathrm{II}3}A_{\mathrm{II}12}\xi^2+A_{\mathrm{II}13}\varphi_{\mathrm{II}1})A_{\mathrm{II}m}e^{-\lambda_{\mathrm{II}1}z}$$
$$+\lambda_{\mathrm{II}2}(\alpha_{\mathrm{II}3}A_{\mathrm{II}12}\xi^2+A_{\mathrm{II}13}\varphi_{\mathrm{II}2})B_{\mathrm{II}m}e^{-\lambda_{\mathrm{II}2}z}\Big]J_m(\xi r)\,d\xi$$
$$\sigma_{\mathrm{II}r\theta m}+(A_{\mathrm{II}11}-A_{\mathrm{II}12})\{(\frac{v_{\mathrm{II}m}}{r})-im(\frac{u_{\mathrm{II}m}}{r})\}=$$
$$-\frac{A_{\mathrm{II}11}-A_{\mathrm{II}12}}{2}\int_0^\infty \xi^3G_{\mathrm{II}m}e^{-\lambda_{\mathrm{II}3}z}J_m(\xi r)\,d\xi$$

(6)

The functions $A_{1m}(\xi)$ to $H_{1m}(\xi)$, $A_{\mathrm{II}m}(\xi)$, $B_{\mathrm{II}m}(\xi)$ and $G_{\mathrm{II}m}(\xi)$ are derived from the boundary and continuity conditions (see Eskandari-Ghadi, et al., 2008).

From the solution given in the previous section, one may find the displacements and stresses Green's functions by replacing the surface loads by point loads as:

$$\mathbf{f}(r,\theta)e^{i\omega t}=\boldsymbol{f}_v(r,\theta)e^{i\omega t}+\boldsymbol{f}_h(r,\theta)e^{i\omega t}\qquad(7)$$

where $\boldsymbol{f}_v(r,\theta)$ and $\boldsymbol{f}_h(r,\theta)$ are, respectively, the vertical and horizontal components of the arbitrary point load, which are defined as:

$$\boldsymbol{f}_v(r,\theta)=\mathscr{F}_v\frac{\delta(r)}{2\pi r}\mathbf{e}_z,\qquad \boldsymbol{f}_h(r,\theta)=\mathscr{F}_h\frac{\delta(r)}{2\pi r}\mathbf{e}_h \tag{8}$$

In addition, $\mathbf{e}_z$ is the vertical unit vector and $\mathbf{e}_h=\mathbf{e}_r\cos\theta-\mathbf{e}_\theta\sin\theta,$ is the horizontal unit vector in arbitrary direction. Therefore

$$\begin{aligned}&P(r,\theta)=\mathscr{F}_h\frac{\delta(r)}{2\pi r}\cos\theta\\&Q(r,\theta)=-\mathscr{F}_h\frac{\delta(r)}{2\pi r}\sin\theta,\quad R(r,\theta)=\mathscr{F}_v\frac{\delta(r)}{2\pi r}\end{aligned} \tag{9}$$

Substituting these relations into the displacements and stresses given in the Eqs. (3) to (6), the related Green's functions are readily given. The point loads given in the Eqs. (9) are applied at the origin. To have the displacements and stresses Green's functions for an arbitrary location of point load, one may use a coordinate transformation to change the place of point load from the origin to an arbitrary surface point $\mathbf{b}=(x_b,y_b,0)$. The required coordinate transformations are (see Figure 1):

$$x'=r\cos\theta-x_b,\quad y'=r\sin\theta-y_b,\quad z=z \tag{10}$$

The inverse relations may be written as:

$$\begin{aligned}&r=\sqrt{x'^2+y'^2}\\&\cos\theta=\frac{x'}{\sqrt{x'^2+y'^2}},\quad \sin\theta=\frac{y'}{\sqrt{x'^2+y'^2}}\end{aligned} \tag{11}$$

The displacements and stresses in the new coordinate system can be explained in terms of the displacements and stresses given in the Eqs. (3) to (6) as:

$$\begin{aligned}&u_{x'}(x',y',z)=u(r,\theta,z)\cos\theta-v(r,\theta,z)\sin\theta\\&u_{y'}(x',y',z)=u(r,\theta,z)\sin\theta+v(r,\theta,z)\cos\theta\\&u_z(x',y',z)=w(r,\theta,z)\\&\sigma_{x'x'}(x',y',z)=\sigma_{rr}(r,\theta,z)\cos^2\theta\\&\quad+\sigma_{\theta\theta}(r,\theta,z)\sin^2\theta-2\sigma_{r\theta}(r,\theta,z)\sin\theta\cos\theta\\&\sigma_{y'y'}(x',y',z)=\sigma_{rr}(r,\theta,z)\sin^2\theta\\&\quad+\sigma_{\theta\theta}(r,\theta,z)\cos^2\theta+2\sigma_{r\theta}(r,\theta,z)\sin\theta\cos\theta\\&\sigma_{x'y'}(x',y',z)=\sigma_{r\theta}(r,\theta,z)(\cos^2\theta-\sin^2\theta)\\&\qquad+\big(\sigma_{rr}(r,\theta,z)-\sigma_{\theta\theta}(r,\theta,z)\big)\sin\theta\cos\theta\\&\sigma_{x'z}(x',y',z)=\sigma_{rz}(r,\theta,z)\cos\theta-\sigma_{\theta z}(r,\theta,z)\sin\theta\\&\sigma_{y'z}(x',y',z)=\sigma_{rz}(r,\theta,z)\sin\theta+\sigma_{\theta z}(r,\theta,z)\cos\theta\\&\sigma_{zz}(x',y',z)=\sigma_{zz}(r,\theta,z)\end{aligned} \tag{12}$$

To have these functions in the original coordinate system, however, with the point loads at $\mathbf{b}=(x_b,y_b,0)$, one needs to replace the relations $(x'=x-x_b,y'=y-y_b,z=z)$ to find:

$$\begin{aligned}&u_x(x,y,z,x_b,y_b)=u(r,\theta,z)\cos\theta-v(r,\theta,z)\sin\theta\\&u_y(x,y,z,x_b,y_b)=u(r,\theta,z)\sin\theta+v(r,\theta,z)\cos\theta\\&u_z(x,y,z,x_b,y_b)=w(r,\theta,z)\\&\sigma_{xx}(x,y,z,x_b,y_b)=\sigma_{rr}(r,\theta,z)\cos^2\theta\\&+\sigma_{\theta\theta}(r,\theta,z)\sin^2\theta-2\sigma_{r\theta}(r,\theta,z)\sin\theta\cos\theta\\&\sigma_{yy}(x,y,z,x_b,y_b)=\sigma_{rr}(r,\theta,z)\sin^2\theta\\&+\sigma_{\theta\theta}(r,\theta,z)\cos^2\theta+2\sigma_{r\theta}(r,\theta,z)\sin\theta\cos\theta\\&\sigma_{xy}(x,y,z,x_b,y_b)=\sigma_{r\theta}(r,\theta,z)(\cos^2\theta-\sin^2\theta)\\&+\big(\sigma_{rr}(r,\theta,z)-\sigma_{\theta\theta}(r,\theta,z)\big)\sin\theta\cos\theta\\&\sigma_{xz}(x,y,z,x_b,y_b)=\\&\qquad\sigma_{rz}(r,\theta,z)\cos\theta-\sigma_{\theta z}(r,\theta,z)\sin\theta\\&\sigma_{yz}(x,y,z,x_b,y_b)=\\&\qquad\sigma_{rz}(r,\theta,z)\sin\theta+\sigma_{\theta z}(r,\theta,z)\cos\theta\\&\sigma_{zz}(x,y,z,x_b,y_b)=\sigma_{zz}(r,\theta,z)\end{aligned} \tag{13}$$

where

$$r = \sqrt{(x - x_b)^2 + (y - y_b)^2}$$
$$\cos\theta = (x - x_b)/r, \qquad \sin\theta = (y - y_b)/r \tag{14}$$

To determine the displacements and stresses for an arbitrary line or patch load, one needs to integrate the displacements and stresses as:

$$\left[\hat{u}_x, \hat{u}_y, \hat{u}_z, \hat{\sigma}_{xx}, ..., \hat{\sigma}_{zz}\right](x, y, z, x_b) = \int_{y_1}^{y_2} \left\{\left[u_x, u_y, u_z, \sigma_{xx}, ..., \sigma_{zz}\right](x, y, z, x_b, y_b)\right\} dy_b \tag{15}$$

$$\left[\hat{u}_x, \hat{u}_y, \hat{u}_z, \hat{\sigma}_{xx}, ..., \hat{\sigma}_{zz}\right](x, y, z) = \iint_{\pi_0} \left\{\left[u_x, u_y, u_z, \sigma_{xx}, ..., \sigma_{zz}\right](x, y, z, x_b, y_b)\right\} dy_b dx_b \tag{16}$$

where the hat is used to illustrate the total displacement or stress function. Furthermore, Eq. (15) gives the displacements and stresses due to a line load applied at x_b from y_1 to y_2 and Eq. (16) gives the same functions due to loads applied on the patch π_0.

NUMERICAL RESULTS

As indicated in Eqs. (3) to (6), the displacements and stresses Green's functions are expressed in terms of one-dimensional semi-infinite integrals. In addition, the total displacements and stresses due to a patch load is a double integral, where the integrand is the Green's function. Thus, volume integrals have to be evaluated to determine the displacements and stresses, where one side of the volume integral is infinite. Because of the presence of radicals, exponential and Bessel functions in a complex form in the integrands, the integrals cannot be given in closed-form. With the aid of the method of residue and contour integration, the semi-infinite integral may be evaluated more accurately. For the numerical evaluation of integrals given in the Eqs. (15) and (16), some careful attention is needed due to the presence of singularities within the range of the integration and the oscillatory nature of the integrands induced by the Bessel functions. The important aspects of the integrands are the branch points and poles. There will be, in general, three branch points at $\xi_{\lambda_{qi}}$, $i = 1, 2, 3$ in each solid domain (Region I and II) lying on the formal path of integration.

There are some poles in the path of integration given in the solutions of Eqs. (3) and (4), which are related to Rayleigh waves at the surface and should be paid special attention. As shown in Figure 1, if the thickness of the top layer goes to infinity or if both regions have the same material properties, the geometry coincides with a half-space subjected to an arbitrary time-harmonic surface load. In this case, there exists one pole related to the Rayleigh wave at the top surface. For a layered medium, however, one should expect the possibility of seeing multiple poles and branch points on the path of integration as in Guzina and Pak (2001). Thus, for evaluating the inner semi-infinite integral one must (i) locate on the ξ-axis all the poles and branch points associated with the branch cuts that render all functions single-valued and consistent with the regularity condition, (ii) integrate from zero to a point in behind the first pole and continuing the integration from a point after the first pole to a point in behind the second pole and so on, and from a point after the last pole to a sufficiently large value, and (iii) adding the contribution from the residue at the pole to the final sum. A detailed investigation for poles ξ_p may be found in (Eskandari-Ghadi et al., 2008).

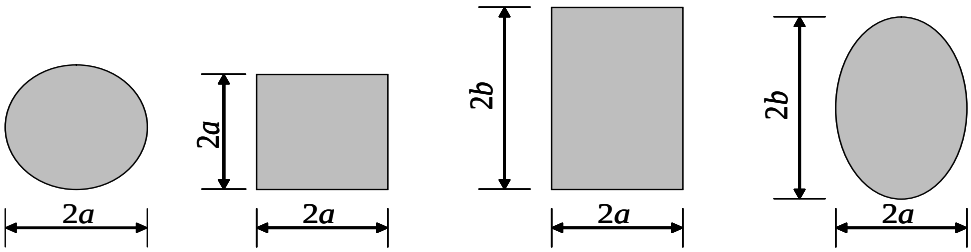

Fig. 2. Different patch at the surface of the domain (see Fig. 1) as loaded area.

Table. 1. Synthetic material engineering constants

Material No.	E (N/mm^2)	E' (N/mm^2)	G (N/mm^2)	G' (N/mm^2)	υ	υ'
I	50000	150000	20000	20000	0.25	0.25
II	100000	50000	40000	20000	0.25	0.25
III	150000	50000	60000	20000	0.25	0.25

If the top layer and the underneath half-space are the same, then there exists only one pole in the integrand, which is related to Rayleigh wave. If the two regions are of different materials, however, then there are two poles, one related to Rayleigh wave at the surface and the other is related to Stoneley wave at the interface. Then, the double integral has to be evaluated to determine the effect of a surface arbitrary shape load. In this study three different shapes, which are circular, rectangular and ellipsoidal, are considered (see Figure 2). The circular patch load is considered to verify the procedure introduced in this study, and the rectangular and the ellipsoidal shape are to present some new numerical results. The surface integrals, in this study, are evaluated with trapezoidal method. Several numerical examples are carried out to illustrate the present solutions for transversely isotropic half-space, with satisfactory results. It needs to be pointed out that all numerical results presented here are dimensionless, with a nondimensional frequency defined as $\omega_0 = a\omega\sqrt{\rho_I / A_{I\,44}}$. The stresses and the displacements are normalized as $\hat{\sigma}_{ij} / \mathscr{F}_I$ and $A_{II\,44}\,\hat{u}_i / a\mathscr{F}_I$ with $i, j = x, y$ and z, and $I = v$ and h.

To illustrate some numerical results, three different materials with the elasticity constants tabulated in Table 1 are selected. The top layer and the underneath half-space is set in such a way the half-space to be always contained Material II, however, the top layer may contain one of the three material listed in Table 1.

Figure 3 illustrates the horizontal displacement $A_{II\,44}\hat{u}_x / a\mathscr{F}_h$ in terms of depth due to horizontal circular patch load of radius a with a dimensionless frequency $\omega_0 = 0.5$ and show a comparison with the results reported by Eskandari-Ghadi et al. (2008), when a layer of Material I with a thickness of $s = a$ rested on a half-space containing Material II. As observed in this figure an excellent agreement can be discovered between the results from this study and Eskandari-Ghadi et al. (2008)[1]. In addition, Figure 4 shows the variation of the stress $\hat{\sigma}_{xz} / \mathscr{F}_h$ in terms of depth due to horizontal circular patch load for a dimensionless frequency $\omega_0 = 0.5$ and also a

[1]The Materials I and II in this study coincide with the Materials II and III in Eskandari-Ghadi et al., (2008)

comparison with Eskandari-Ghadi et al., (2008)[2]. for the set of layer and half-space as in Figure 1. Again a very good agreement can be seen in this figure. Figures 5 and 6 illustrate the horizontal displacement and the shear stress due to a rectangular patch load with $b = 2a$ (see Figure 2) for a low frequency of $\omega_0 = 0.5$, and Figures 7 and 8 show the same functions due to a square patch load of length $2a$ for a high frequency of $\omega_0 = 3.0$, where three different configurations of top layer and half-space as mentioned before are considered. In all cases, the thickness of the half-space is considered to be equal to a. The radiation condition is clearly satisfied, and the wave length shows the wave number of both the displacements and stresses. The high value of displacement in the configuration of Material I and Material II is clear from the values listed in Table 1.

Figures 9 and 10 depict the vertical displacement and the axial stress $\hat{\sigma}_{zz}$ in terms of depth due to an elliptical vertical patch load for three sets of top layer and half-space for a high frequency time harmonic load. The dimensions of ellipsoid are selected in such a way its area to be the same as the area of the previous rectangular patch. As seen the radiation condition are satisfied very clearly. Figures 11 to 14 show the vertical displacement and the stress $\hat{\sigma}_{zz}$ for vertical load applied on a square for low and high frequency. Figures 15 and 16 depicts the vertical displacement and the axial stress $\hat{\sigma}_{zz}$ in terms of depth due to a rectangular vertical patch load for three sets of top layer and half-space for a high frequency time harmonic load.

To compare the displacements and stresses due to different patch load, the vertical displacement and the stress $\hat{\sigma}_{zz}$ due to ellipsoidal and rectangular vertical patch load are compared in Figures 17 to 20. As observed in these figures, the same trend and the same amplitude for the displacements and stresses are seen. Satisfying the Saint Venant's principle is clear here in the figures. As illustrated in Figures 17 to 20, the static and the dynamic cases of principle of Saint Venant are different. In the static case, the value of the displacement/stress and its place are the same, while in dynamic case the amplitude of the function is the same.

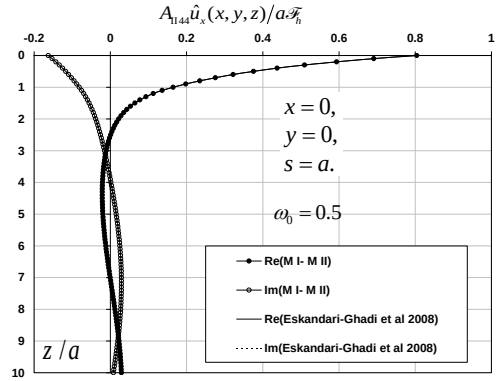

Fig. 3. Horizontal displacement in terms of depth due to horizontal circular patch load with a dimensionless frequency $\omega_0 = 0.5$ and comparison with Eskandari-Ghadi et al. (2008).

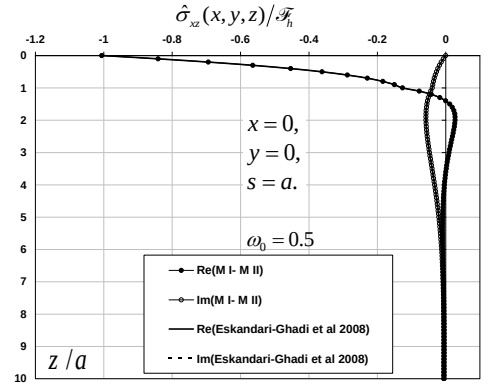

Fig. 4. The stress $\hat{\sigma}_{xz}$ in terms of depth due to horizontal circular patch load with a dimensionless frequency $\omega_0 = 0.5$ and comparison with Eskandari-Ghadi et al. (2008).

[2] The results in Eskandari-Ghadi et al., (2008). have been modified in such a way to be comparable with the results here.

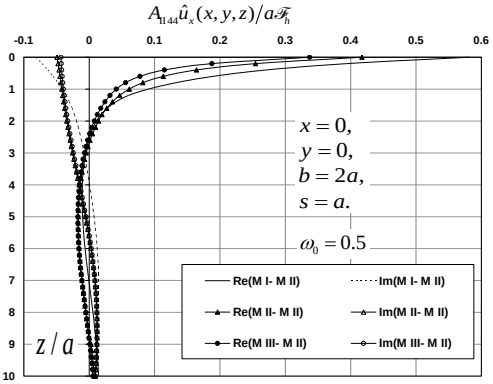

Fig. 5. Horizontal displacement in terms of depth due to horizontal ellipsoidal patch load with a dimensionless frequency $\omega_0 = 0.5$.

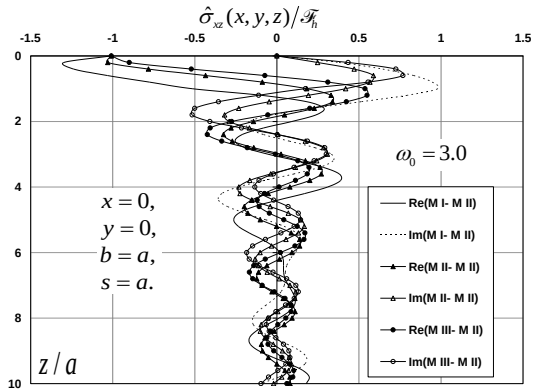

Fig. 8. The stress $\hat{\sigma}_{xz}$ in terms of depth due to horizontal square patch load with a dimensionless frequency $\omega_0 = 0.5$.

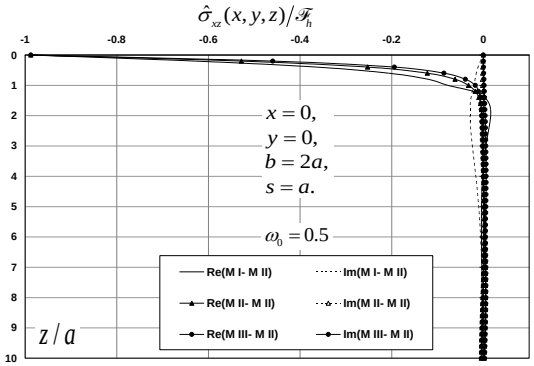

Fig. 6. The stress $\hat{\sigma}_{xz}$ in terms of depth due to horizontal ellipsoidal patch load with a dimensionless frequency $\omega_0 = 0.5$.

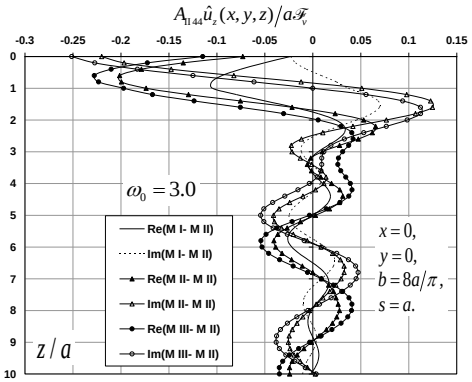

Fig. 9. Vertical displacement in terms of depth due to vertical ellipsoidal patch load with a dimensionless frequency $\omega_0 = 3.0$.

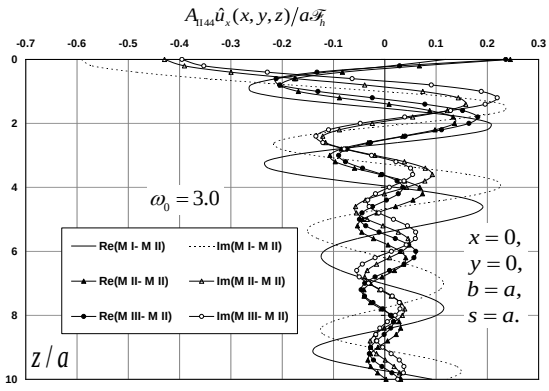

Fig. 7. Horizontal displacement in terms of depth due to horizontal square patch load with a dimensionless frequency $\omega_0 = 3.0$.

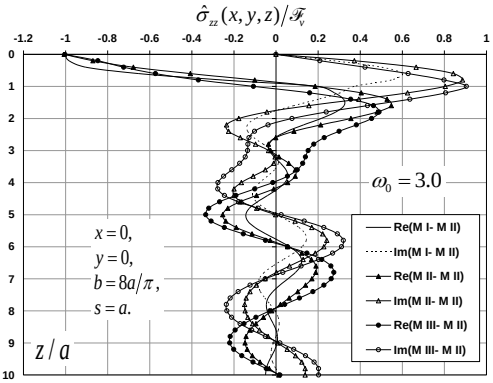

Fig. 10. The stress $\hat{\sigma}_{zz}$ in terms of depth due to vertical ellipsoidal patch load with a dimensionless frequency $\omega_0 = 3.0$.

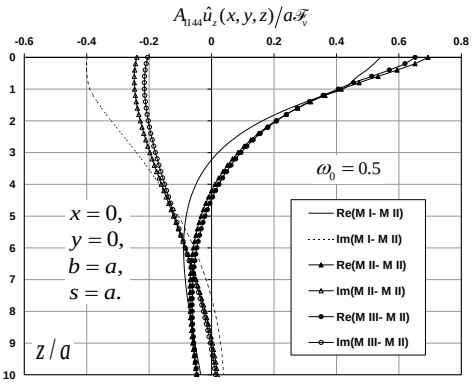

Fig. 11. Vertical displacement in terms of depth due to vertical square patch load with a dimensionless frequency $\omega_0 = 0.5$.

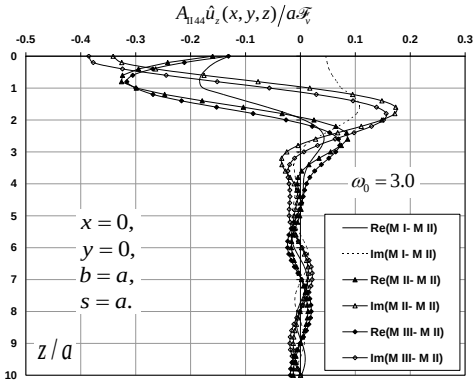

Fig. 14. Vertical displacement in terms of depth due to vertical square patch load with a dimensionless frequency $\omega_0 = 3.0$.

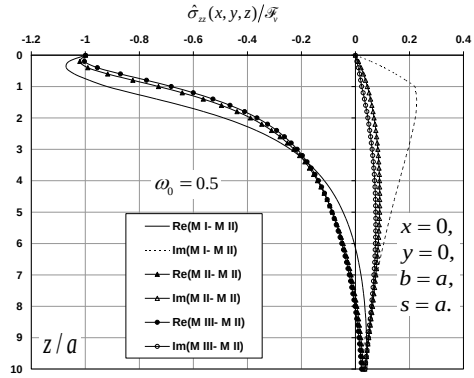

Fig. 12. The stress $\hat{\sigma}_{zz}$ in terms of depth due to vertical square patch load with a dimensionless frequency $\omega_0 = 0.5$.

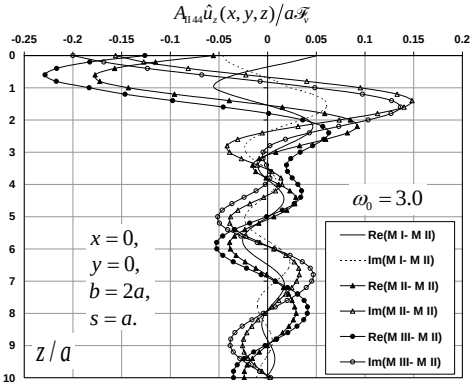

Fig. 15. Vertical displacement in terms of depth due to vertical rectangular patch ($b = 2a$) load with a dimensionless frequency $\omega_0 = 3.0$.

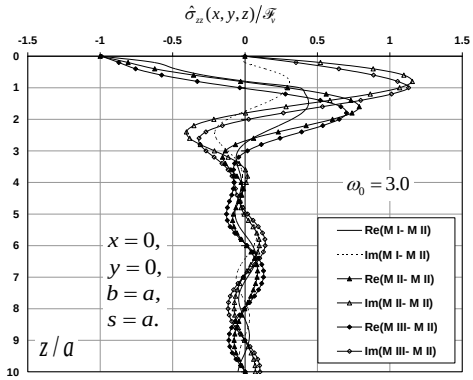

Fig. 13. The stress $\hat{\sigma}_{zz}$ in terms of depth due to vertical square patch load with a dimensionless frequency $\omega_0 = 3.0$.

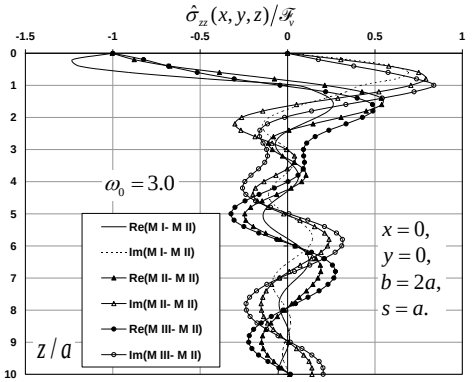

Fig. 16. The stress $\hat{\sigma}_{zz}$ in terms of depth due to vertical rectangular patch ($b = 2a$) load with a dimensionless frequency $\omega_0 = 3.0$.

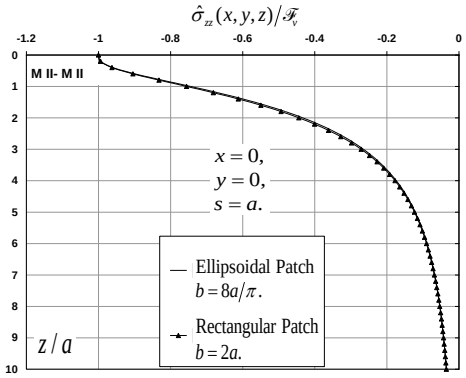

Fig. 17. Comparison of the stress $\hat{\sigma}_{zz}$ due to ellipsoidal and rectangular vertical patch load in the static case, $\omega_0 = 0$.

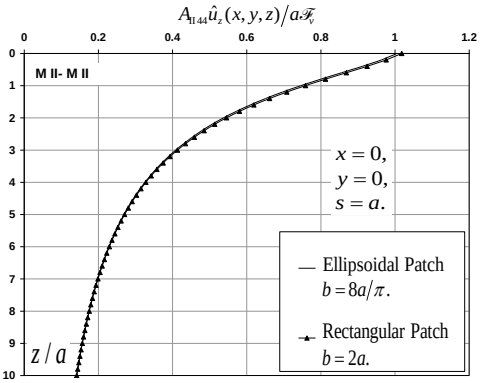

Fig. 18. Comparison of the vertical displacement due to ellipsoidal and rectangular vertical patch load in the static case, $\omega_0 = 0.$

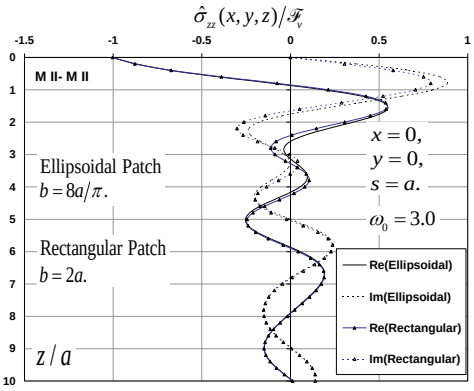

Fig. 19. Comparison of the stress $\hat{\sigma}_{zz}$ due to ellipsoidal and rectangular vertical patch load with a dimensionless frequency $\omega_0 = 3.0$.

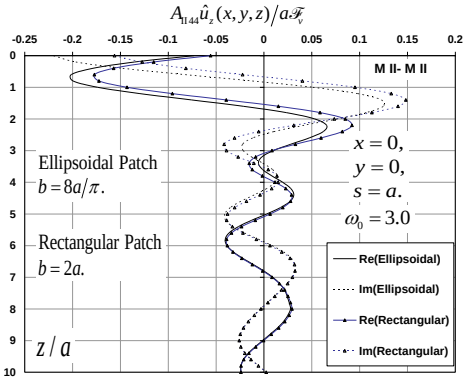

Fig. 20. Comparison of the vertical displacement due to ellipsoidal and rectangular vertical patch load with a dimensionless frequency $\omega_0 = 3.0$.

CONCLUSIONS

The effect of an arbitrary shape surface horizontal and vertical time harmonic load on response of a transversely isotropic, linearly elastic half-space containing a top layer with different mechanical properties have been analytically investigated in this paper. With the help of displacements and stresses Green's functions, an analytical formulation has been presented in the form of double integrals for determination the displacements and stresses at any point in the domain of the problem. The numerical evaluation has been done with special attention and an excellent agreement has been obtained, when compared with existing results. Some new results have been presented for ellipsoidal, square and rectangular patch load. It is shown that the static and the dynamic cases of Saint Venant's principle are different.

NOTATION

A_{qij} = elasticity constants of the q[th] region
a = half of the maximum dimension of surface force in x-direction
b = half of the maximum dimension of surface force in y-direction

E = Young's moduli in the plane of transverse isotropy

E' = Young's moduli in the direction normal to the plane of transverse isotropy

G = shear modulus in the plane normal to the axis of symmetry

G' = shear modulus in planes normal to the plane of transverse isotropy

J_m = Bessel function of the first kind and m[th] order

$P(r,\theta)$ = time-harmonic surface force component in r-direction

$Q(r,\theta)$ = time-harmonic surface force component in θ-direction

$R(r,\theta)$ = time-harmonic surface force component in z-direction

π_0 = arbitrary patch of load at $z=0$

$\mathcal{F}_h\delta(r)/2\pi r$ = point horizontal load of magnitude $\mathcal{F}_h$

$\mathcal{F}_v\delta(r)/2\pi r$ = point vertical load of magnitude $\mathcal{F}_v$

e_h = unit vector in horizontal plane

e_z = unit vector in z-direction

e_r = unit vector in r-direction

e_θ = unit vector in θ-direction

r = radial coordinate

s = thickness of region I in z-direction

t = time variable

u = displacement component in r-direction

$\hat{u}_i, u_i (i = x, y, z)$ = displacement component in i-direction in Cartesian coordinate system

v = displacement component in θ-direction

w = displacement component in z-direction

$(x, y, z), (x', y', z)$ = Cartesian coordinate systems

$\mathbf{b}(x_b, y_b, 0)$ = location of point load in Cartesian coordinate system

z = vertical coordinate

$\delta(r)$ = Dirac-delta function

$\varepsilon_{ij}(i, j = r, \theta, z)$ = strain components

θ = angular coordinate

λ = Lame's constant

λ_{q1}, λ_{q2} , λ_{q3} = radicals appearing in general solutions

μ = Lame's constant

υ = Poisson's ratios characterizing the lateral strain response in the plane of transverse isotropy to a stress acting parallel to it

υ' = Poisson's ratios characterizing the lateral strain response in the plane of transverse isotropy to a stress acting normal to it

ξ = Hankel's parameter

$\xi_{\lambda_{q1}}, \xi_{\lambda_{q2}}, \xi_{\lambda_{q3}}, \xi_p$ = branch points and simple pole on positive real axis

ρ = material density

$\sigma_{ij}(i, j = r, \theta, z)$ = stress tensor in polar coordinate system

$\hat{\sigma}_{ij}, \sigma_{ij}(i, j = x, y, z)$ = stress tensor in Cartesian coordinate system

ω_0 = nondimensional frequency

ω = angular frequency

ACKNOWLEDGEMENT

The second author (M. E.-G.) would like to acknowledge the financial support from the University of Tehran for this research under grant number 27840/01/04.

REFERENCES

Ahmad, S. and Rupani, A.K. (1999). "Horizontal impedance of square foundation in layered soil", *Soil Dynamics and Earthquake Engineering*, 18(1), 59-69.

Algin, H.M. (2000). "Stresses from linearly distributed pressures over rectangular areas", *International Journal for Numerical and Analytical Methods in Geomechanics*, 24(8), 681 – 692.

Bycroft, G.N. (1980). "Soil-foundation interaction and differential ground motions", *Earthquake Engineering & Structural Dynamics*, 8(5), 397–404.

Dhawan, G.K. (1979). "Transversely isotropic half-space indented by a flat annular rigid stamp", *ACTA MECHANICA*, 31(3-4), 291-299.

Egorov, K.E. (1965). "Calculations of bed for foundation with ring footing", *Proc. 6th International Conference of Soil Mechanics and Foundation Engineering*, 2, 41-45.

Eskandari-Ghadi, M., Pak, R.Y.S. and Ardeshir-Behrestaghi, A. (2008). "Transversely isotropic elastodynamic solution of a finite layer on an infinite subgrade under surface loads", *Soil Dynamics and Earthquake Engineering*, 28, 986-1003.

Eskandari-Ghadi. M., Pak, R.Y.S. and Ardeshir-Behrestaghi, A. (2009). "Elastostatic green's functions for an arbitrary internal load in a transversely isotropic bi-material full-space", *International Journal of Enginering Science*, 47(4), 631-641.

Guzina, B.B. and Nintcheu, F.S. (2001). "Axial vibration of a padded annulus on a semi-infinite viscoelastic medium", *Journal of Applaied Mechanics, ASME*, 68(6) 923–928.

Guzina, B.B. and Pak, R.Y.S. (2001). "On the analysis of wave motions in a multi- layered solid", *The Quarterly Journal of Mechanics & Applied Mathematics*, 54(1), 13–37.

Harding, J.W. and Sneddon, I.N. (1945). "The elastic stresses produced by the indentation of the plane surface of a semi-infinite elastic solid by a rigid punch", *Mathematical Proceedings of the Cambridge Philosophical Society*, 41, 16-26.

Iguchi, M. and Luco, J.E. (1980). "Dynamic response of flexible rectangular foundations on an elastic half-space", *Earthquake Engineering & Structural Dynamics*, 9(3), 239 – 249.

Johnson, J.L. (1986). *Contact Mechanics*, Cambridge University. Press.

Keer, L.M. (1967). "Mixed boundary value problems for an elastic half-space", *Mathematical Proceedings of the Cambridge Philosophical Society*, 63, 1379-1386.

Kenzo, S. (2000). "Buckling of a clamped elliptical plate on the elastic foundation under uniform compression", *Transactions of the Japan Society of Mechanical Engineers*, 66(649), 1751-1757.

Kim, K., Roesset, J.M. and Tassoulas, J.L. (1987). "Interaction between concentric annular and circular foundations", *Journal of Geotechnical Engineering*, 113(6), 555–567.

Lekhnitskii , S.G. (1981). *Theory of anisotropic elastic bodies*, Holden-Day Publishing Co, San Francisco, Calif.

Melerski, E.S. (1997). "Numerical modeling of elastic interaction between circular rafts and cross anisotropic media", *Computers & Structures*, 64(1-4), 567–78.

Mita, A. and Luco, J.E. (1989). "Dynamic response of a square foundation embedded in an elastic half-space", *Soil Dynamics and Earthquake Engineering*, 8(2), 54-67.

Pak, R.Y.S., Simmons B.M. and Ashlock, J.C. (2008). "Tensionless contact of a flexible plate and annulus with a smooth half-space by integral equations", *International Journal of Mechanical Sciences*, 50, 1004–1011.

Shield, T.W. and Bogy, D.B. (1989). "Some axisymmetric problems for layered elastic media. II: solutions for annular indenters and cracks", *Journal of Applied Mechanics*, 56, 807-813.

Tassoulas, J.L. and Kausel, E. (1984). "On the dynamic stiffness of circular ring footings on an elastic stratum", *International Journal for Numerical and Analytical Methods in Geomechanics*, 8(5), 411-426.

Veletsos, A.S. and Tang, Y. (1987). "Vertical vibration of ring foundations", Earthquake Engineering & Structural Dynamics, 15(1), 1–21.

Veletsos, A.S., Prasad, A.M. and Wu, W.H. (1996). "Transfer functions for rigid rectangular foundations", *Earthquake Engineering & Structural Dynamics*, 26(1), 5–17.

Wong, H.L. and Luco, J.E. (1976). "Dynamic response of rigid foundations of arbitrary shape", *Earthquake Engineering & Structural Dynamics*, 4(6), 579 – 587.

Wong, H.L. and Trifunac, M.D. (1974) "Interaction of a shear wall with the soil for incident plane SH waves: elliptical rigid foundation", *Bulletin of the Seismological Society of America*, 64(6), 1825-1842.